



**HAL**  
open science

## Understanding the $\text{Cu}^{2+}$ adsorption mechanism on activated carbon using advanced statistical physics modelling

Lotfi Sellaoui, Fatma Dhaouadi, Sonia Taamalli, Florent Louis, Abderrahman El Bakali, Michael Badawi, Adrián Bonilla-Petriciolet, Luis Silva, Kátia da Boit Martinello, Guilherme Luiz Dotto, et al.

### ► To cite this version:

Lotfi Sellaoui, Fatma Dhaouadi, Sonia Taamalli, Florent Louis, Abderrahman El Bakali, et al.. Understanding the  $\text{Cu}^{2+}$  adsorption mechanism on activated carbon using advanced statistical physics modelling. *Environmental Science and Pollution Research*, 2022, 29, pp.54882-54889. 10.1007/s11356-022-19795-7. hal-03633260

**HAL Id: hal-03633260**

**<https://hal.science/hal-03633260>**

Submitted on 19 Jan 2024

**HAL** is a multi-disciplinary open access archive for the deposit and dissemination of scientific research documents, whether they are published or not. The documents may come from teaching and research institutions in France or abroad, or from public or private research centers.

L'archive ouverte pluridisciplinaire **HAL**, est destinée au dépôt et à la diffusion de documents scientifiques de niveau recherche, publiés ou non, émanant des établissements d'enseignement et de recherche français ou étrangers, des laboratoires publics ou privés.



26 models contain parameters that were utilized to provide new insights into the possible  
27 adsorption mechanism at the molecular scale. In particular, a monolayer adsorption model was  
28 the best alternative to correlate the  $\text{Cu}^{2+}$  adsorption data at 25 – 55 °C and pH 5.5. Furthermore,  
29 the application of this model for copper adsorption data analysis showed that the removal of this  
30 heavy metal ion was a multi-cationic process. This theoretical finding indicated that  $\text{Cu}^{2+}$  ions  
31 interacted via one functional group of activated carbon surface during adsorption. In this  
32 direction, the adsorption energy was calculated thus showing that  $\text{Cu}^{2+}$  removal was endothermic  
33 and associated with physical interaction forces. Furthermore, these activated carbons showed  
34 saturation adsorption capacities from 54.6 to 87.0 mg/g for  $\text{Cu}^{2+}$  removal, and their  
35 performances outperformed other adsorbents available in the literature. Overall, these results  
36 provided new insights of the adsorption mechanism of this water pollutant using activated carbons.

37

38 **Keywords:** Adsorption; Copper; Isotherms; Statistical physics;

39

## 40 **1. Introduction**

41

42 Copper is a transition metal, electrically and thermally conductive, but it is also considered as  
43 an environmental pollutant (Kayalvizhi et al. 2022). Natural disasters (e.g., volcanic phenomena)  
44 and anthropogenic activities (e.g., metal industries, tanning factories, and automobile  
45 industries) contribute to the pollution caused by copper. This metal is toxic even at relatively  
46 low concentrations, and, consequently, the highest permissible concentration level of copper  
47 ions ( $\text{Cu}^{2+}$ ) in marine water has been established as 4.8  $\mu\text{g/L}$ . In comparison, the maximum  $\text{Cu}^{2+}$   
48 concentration for drinking water is 1300  $\mu\text{g/L}$ , as reported by the WHO and EPA (Katiyar et al.  
49 2021; Kayalvizhi et al. 2022). Chronic exposure to this metal can affect vital organs such as the

50 intestines, stomach, and liver. It can also generate diverse symptoms such as liver disease,  
51 gallbladder, and metabolic disturbances(Dou et al. 2019; Sun et al. 2022).

52         Consequently, the drinking water resources and effluents polluted with  $\text{Cu}^{2+}$  must be  
53 treated to reduce their concentration thus avoiding environmental impacts and to protect human  
54 health. Various procedures have been reported to remove  $\text{Cu}^{2+}$  ions from liquid phase. They  
55 include ion exchange, precipitation, electrolysis, reverse osmosis, flocculation, biochemical  
56 methods, and membrane-based filtration (Godiya et al. 2019; Nyström et al. 2020; Anbazhagan  
57 et al. 2021; Lemes and Tarley 2021). However, these removal methods have disadvantages such  
58 as unfavorable cost-effectiveness tradeoffs or the generation of toxic sediments and wastes(e.g.,  
59 sludge)(Rukayat et al. 2021). In contrast, the adsorption process is a competitive technique  
60 compared to other methods due to its ease of handling, low cost, and removal efficacy even at  
61 low concentrations of heavy metal ions (Vocciante et al. 2014; Pan et al. 2019; Khan et al.  
62 2021). Activated carbon is the most employed adsorbent in this process because it effectively  
63 removes inorganic and organic pollutants from wastewaters and industrial effluents. This  
64 adsorbent outperforms other materials reported for water treatment in terms of its production  
65 cost and the availability of a wide spectrum of preparation routes that is already exploited and  
66 commercialized at large industrial scale. The adsorption performance of activated carbon is  
67 governed by its pore structure and surface chemistry. The modification of activated carbon is  
68 aimed to optimize these properties (Bell et al. 2011), and this adsorbent can be obtained from  
69 different feedstock and preparation conditions, thus affecting its adsorption properties. Surface  
70 functionalization of activated carbons can be performed with several chemicals to tailor their  
71 performance for the removal of target pollutants.

72         Under this context, citric wastes can be an option to produce activated carbons since  
73 they are generated in large amounts by industries of juices and jams. During the production  
74 process of juices and jams, around 50-60% of the entire citric fruit is discarded. These wastes

75 cannot be released into the environment since they generate CH<sub>4</sub>. On the other hand, they are  
76 rich in lignin, cellulose, hemicellulose, and pectin, thus being an attractive feedstock for  
77 pyrolysis and their conversion into activated carbon (Lam et al. 2016, 2018).

78 The modeling of adsorption data of heavy metals and other water pollutants is important  
79 for water treatment design. Therefore, it is possible to apply classical models (e.g., Langmuir)  
80 to theoretically study the adsorption data. Unfortunately, this and other traditional models are  
81 not useful to understand the adsorption mechanisms due to the limitations in their hypotheses.  
82 For instance, Langmuir model considers that each functional group can accept one ion for all  
83 adsorption systems. This assumption is an obstacle to provide proper interpretations of more  
84 complex adsorption mechanisms. The application of reliable models to analyze and explain the  
85 adsorption of heavy metal ions on activated carbon surfaces is paramount to develop effective  
86 and low-cost water treatment methods.

87 In this research, two homogeneous and heterogeneous models based on statistical  
88 physics theory were implemented to explain the adsorption mechanism of Cu<sup>2+</sup> on a set of  
89 activated carbons obtained from different citric wastes namely orange (OP), tangerine (MP),  
90 lemon (RLP) and lime (SLP). These models allowed to analyze the adsorption mechanism at  
91 the microscopic scale. New insights on steric and energetic parameters that governed the  
92 removal of this relevant water pollutant were developed for all tested activated carbons.

93

## 94 **2. Description of experimental isotherms and statistical physics models**

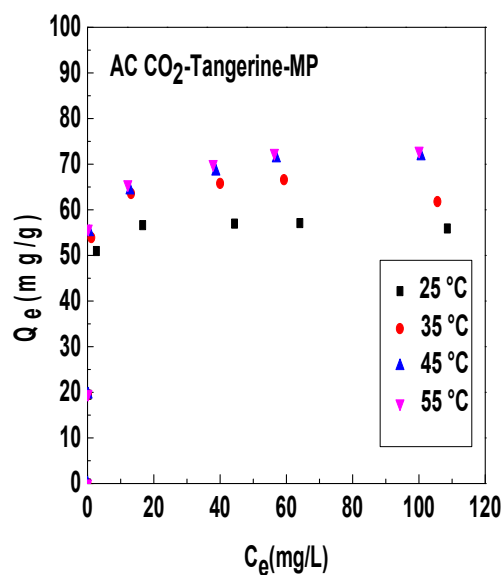
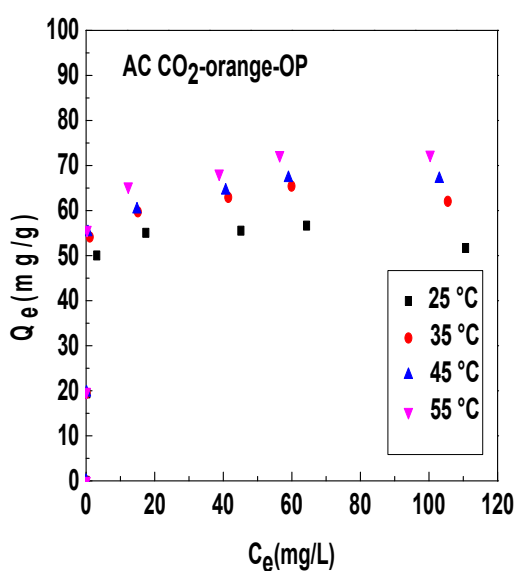
95

### 96 *2.1. Preparation of AC and quantification of Cu<sup>2+</sup> adsorption isotherms*

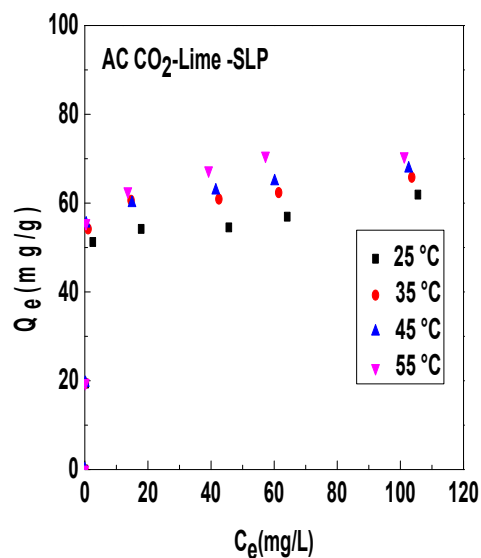
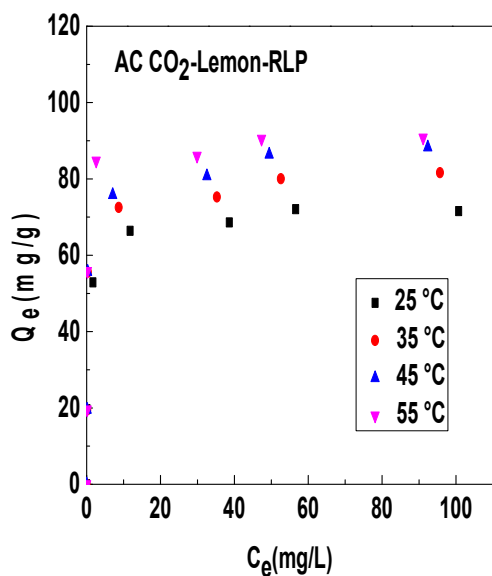
97

98 Cu<sup>2+</sup> adsorption isotherms were quantified with four activated carbons prepared from citrus  
99 waste (Dotto et al. 2011; Perondi et al. 2017). For the adsorbent preparation, 100 g of each citrus

100 waste werelocated in a stainless reactor of 127 x 8.5 cm. The reactor was heated at 5 °C/min  
 101 until 900 °C and remained at this temperature for 15 min. Then, the system was cooled until  
 102 ambient temperature. All these steps were performed with N<sub>2</sub> flowof 0.2 L/min. Subsequently,  
 103 the N<sub>2</sub> flow was replaced by CO<sub>2</sub> flow (2 kg/h for 15 min). Finally, the adsorbent samples were  
 104 removed from the reactor, washed and used in adsorption experiments. These adsorbents were  
 105 labelled as AC CO<sub>2</sub>-orange-OP, AC CO<sub>2</sub>-tangerine-OP,AC CO<sub>2</sub>-lemon-RLP and AC CO<sub>2</sub>-  
 106 Lime-SLP.



107



108

109 **Figure 1:** Experimental isotherms of the adsorption of  $\text{Cu}^{2+}$  ions on different activated carbons  
110 at 25-55 °C and pH 5.5.

111

112 Typical batch equilibrium experiments were performed to obtain the  $\text{Cu}^{2+}$  adsorption  
113 isotherms. Aqueous solutions (50 mL) with different initial  $\text{Cu}^{2+}$  concentrations up to 150 mg/L  
114 were prepared from copper sulfate and the solution pH was adjusted to 5.5. Next, these solutions  
115 were placed in Erlenmeyer flasks located in a thermostated shaker. Adsorption isotherms were  
116 quantified at 25, 35, 45 and 55 °C using an activated carbon dosage of 0.5 g/L under constant  
117 stirring of 200 rpm for 5 h. The solid-liquid separation was performed by centrifugation and  
118  $\text{Cu}^{2+}$  concentration in the liquid was quantified by flame atomic absorption  
119 spectroscopy. Then, the equilibrium adsorption capacities were calculated via a mass balance for  
120 a stirred tank using the initial and final  $\text{Cu}^{2+}$  concentrations used in the experiments and the  
121 corresponding adsorbent dosage. Figure 1 shows the experimental isotherms of  
122  $\text{Cu}^{2+}$  adsorption on the four activated carbons analyzed in this paper.

123 Solution temperature positively affected all adsorbed quantities of  $\text{Cu}^{2+}$  ions on these  
124 activated carbons, thus suggesting an endothermic removal process. All experimental isotherms  
125 followed the monotonic trend of adsorbed  $\text{Cu}^{2+}$  quantities as a function of equilibrium  
126 concentration until the saturation region was reached. This adsorbent saturation was caused by  
127 forming a layer of  $\text{Cu}^{2+}$  ions adsorbed on the surfaces of tested activated carbons. In this  
128 regard, homogeneous and heterogeneous monolayer models developed from statistical physics  
129 theory were implemented to analyze  $\text{Cu}^{2+}$  adsorption isotherms at the microscopic scale. The  
130 next two scenarios were tested in this modeling study:

131 **Scenario 1:** A homogeneous monolayer model (HMM) was considered where only one type of  
132 functional group participated in the adsorption of  $\text{Cu}^{2+}$  ions on tested adsorbents. It was assumed  
133 that only one adsorption energy was involved in the metal ion removal, which represented the

134 interaction of  $\text{Cu}^{2+}$  ion-activated carbon surface. The adsorbed quantity calculated with this  
135 model is given by (Sellaoui et al. 2018; Dhaouadi et al. 2020c, b, a):

136

137

$$Q_e = \frac{nS_m}{1 + \left(\frac{C_{1/2}}{C_e}\right)^n} \quad (1)$$

138

139 **Scenario 2:** A heterogeneous monolayer model (IMM) was also applied. Two functional  
140 groups participated in the adsorption of  $\text{Cu}^{2+}$  ions with two different adsorption energies:  $\text{Cu}^{2+}$   
141 ion – adsorption site 1 and  $\text{Cu}^{2+}$  ion– adsorption site 2. In this model, the adsorbed quantity as a  
142 function of the equilibrium concentration is defined as (Dhaouadi et al. 2020b, a, 2021):

143

144

$$Q_e = \frac{n_1 S_{m1}}{1 + \left(\frac{C_1}{C_e}\right)^{n_1}} + \frac{n_2 S_{m2}}{1 + \left(\frac{C_2}{C_e}\right)^{n_2}} \quad (2)$$

145

146 For these models,  $n$  and  $n_i (i=1, 2)$  are the numbers of  $\text{Cu}^{2+}$  ions adsorbed per functional group(s),  
147  $S_m$  and  $S_{mi}$  are the densities of these surface functionalities,  $C_{1/2}$  and  $C_i (i=1, 2)$  are the  
148 concentrations at half-saturation, respectively.

149

150 Characterization results showed that these activated carbons contained different  
151 functional groups that can contribute to the adsorption of  $\text{Cu}^{2+}$  ions. Therefore, these adsorption  
152 models were consistent with the surface chemistry of these activated carbons. Note that  
153 these models were developed by applying a grand canonical ensemble of statistical physics with  
154 the aim of obtaining a better analysis of the adsorption mechanism of this pollutant. Overall,  
155 these models assumed that the adsorption of  $\text{Cu}^{2+}$  ions was a monolayer process, but with the  
contribution of one (homogeneous monolayer model) and two (heterogeneous monolayer



156 model) functional groups in the removal of this cation(Dhaouadi et al. 2020b, 2021).In  
 157 summary, these models can describe the role of these functional groups on the adsorption of  
 158 this metallic ion andcan also characterize the nature of their interactions (i.e., multi-interaction  
 159 or multi-ionic process).

160

161

162

163

164

165

166

167

168

169

170 **Table 1:** Results of the Cu<sup>2+</sup>adsorption isothermcorrelation with a homogeneous monolayer  
 171 model.

172

173

<i>T</i> (°C)	<i>R</i> <sup>2</sup>	<i>n</i>	<i>S<sub>m</sub></i> (mg/g)	<i>C</i> <sub>1/2</sub> (mg/L)	<i>Q<sub>s</sub></i> (mg/g)
<b>AC CO<sub>2</sub>- Orange-OP</b>					
<b>25</b>	0.992	1.13	48.35	0.38	54.63
<b>35</b>	0.994	1.46	42.61	0.31	62.21
<b>45</b>	0.989	1.70	37.88	0.19	64.39
<b>55</b>	0.977	1.82	37.49	0.07	68.23
<b>AC CO<sub>2</sub>- Tangerine-MP</b>					

25	0.999	1.07	53.20	0.35	56.92
35	0.995	1.24	51.80	0.32	64.23
45	0.989	1.83	37.65	0.27	68.89
55	0.990	4.20	16.71	0.14	70.18
<b>AC CO<sub>2</sub>- Lemon-RLP</b>					
25	0.998	0.63	115.75	0.39	72.92
35	0.987	2.88	26.85	0.25	77.32
45	0.984	2.90	28.55	0.22	82.79
55	0.994	4.55	19.32	0.18	87.90
<b>AC CO<sub>2</sub>-Lime-SLP</b>					
25	0.984	1.15	49.55	0.44	56.98
35	0.993	1.56	40.03	0.31	62.44
45	0.988	3.04	20.96	0.238	63.71
55	0.988	3.16	21.42	0.232	67.68

174

175           These models were employed to fit all Cu<sup>2+</sup> ion adsorption isotherms, and their  
176 parameters were determined via a multivariable nonlinear regression with the Levenberg-  
177 Marquardt method. Determination coefficients ( $R^2$ ) and the trends of steric and energetic  
178 parameters indicated that the HMM model was the most suitable for analyzing the Cu<sup>2+</sup> removal  
179 at the microscopic scale. Table 1 provides the results of Cu<sup>2+</sup> adsorption data fitting for the  
180 HMM model and their corresponding steric and energetic parameters for tested experimental  
181 conditions. In addition, the fitting of Cu<sup>2+</sup> adsorption isotherms by the HMM model is illustrated  
182 in the appendix.

183

184 **3. Results and discussion**

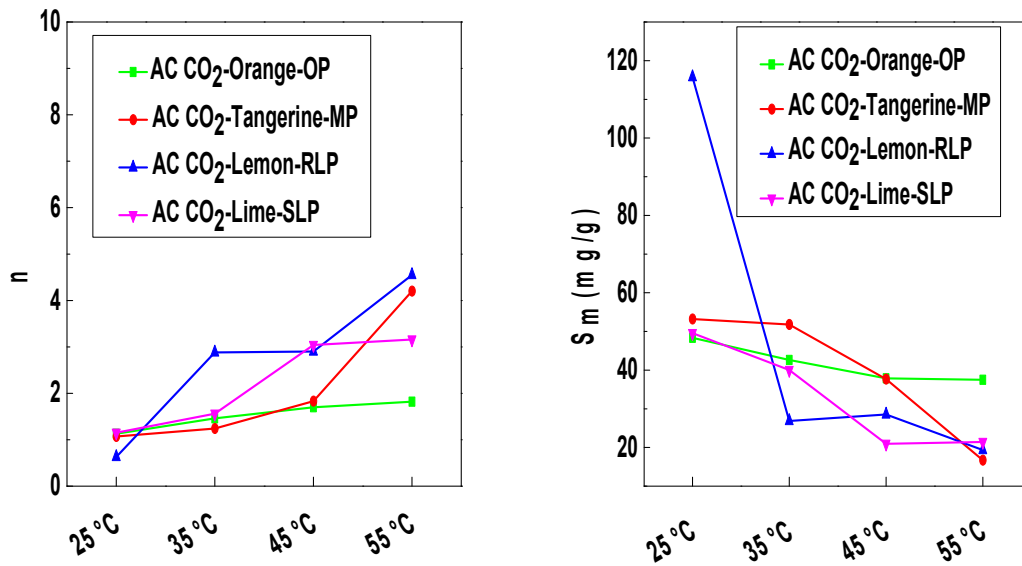
185

186 *3.1. Evaluation of the number of Cu<sup>2+</sup> ions adsorbed per functional group and their adsorption*  
187 *site densities*

188

189 The impact of temperature on the number of adsorbed Cu<sup>2+</sup> ions per functional group and their  
190 corresponding adsorption site densities for these activated carbons is represented in Figure 2.

191 All parameters  $n$  were higher than unity except for AC CO<sub>2</sub>-Lemon-RLP adsorbent at 25  
192 °C. This result indicated that the adsorption of this heavy metal was multi-cationic for these  
193 activated carbons, where the functional groups could adsorb several cations  
194 simultaneously (Dhaouadi et al. 2020b, a). Indeed, the exceptional case (i.e.,  $n=0.63$ ) showed  
195 that Cu<sup>2+</sup> ions could be adsorbed on the surface of AC CO<sub>2</sub>-Lemon-RLP via a combined  
196 interaction where one and two functional groups can participate in the removal with two  
197 different proportions (Dhaouadi et al. 2021). Thermally speaking, the temperature increased the  
198 number of Cu<sup>2+</sup> ions adsorbed per functional group from 1.13 to 1.82, 1.07 to 4.20, 0.63 to 4.59,  
199 and 1.15 to 3.16 for the adsorbents AC CO<sub>2</sub>-Orange-OP, AC CO<sub>2</sub>-Tangerine-MP, AC CO<sub>2</sub>-  
200 Lemon-RLP and AC CO<sub>2</sub>-Lime-SLP, respectively. Overall, these results indicated that the  
201 temperature played a relevant role to adsorb the Cu<sup>2+</sup> ions.



202

203 **Figure 2:** Impact of temperature on the parameters  $n$  and  $S_m$  for the  $\text{Cu}^{2+}$  adsorption at pH 5.5  
 204 using different activated carbons.

205

206 Figure 2 indicated that the density of functional groups of these activated carbons  
 207 reduced as a function of temperature. Moreover, this tendency was inversely proportional to the  
 208 number of  $\text{Cu}^{2+}$  ions adsorbed per functional group. Thus, the increment of the parameter  $n$  as a  
 209 function of temperature suggested a reduction of the occupied functional groups and,  
 210 consequently, a decrement of the adsorption density and vice versa.

211

### 212 3.2. Performance evaluation of different activated carbons for $\text{Cu}^{2+}$ adsorption

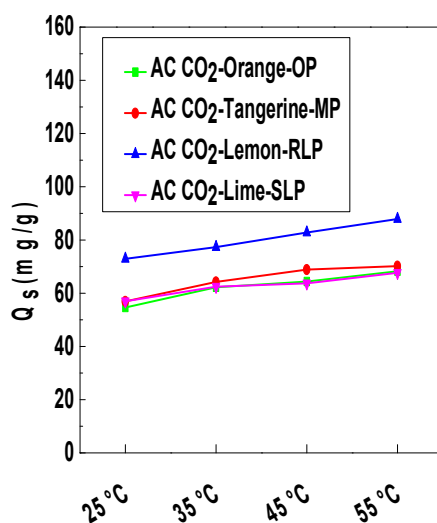
213

214 The performance of tested adsorbents was complemented via the calculation of adsorption  
 215 capacities at saturation using the next expression:

216

$$Q_s = nS_m \quad (3)$$

217 The impact of thermal agitation on the adsorbed quantity at saturation  $Q_s$  for the different  
 218 adsorbents is given in Figure 3.



219

220 **Figure 3:** The adsorbed quantity of Cu<sup>2+</sup> ions at saturation as a function of temperature for  
 221 different activated carbons at pH 5.5.

222

223 Figure 3 indicated that the adsorbed quantity at saturation for the four activated carbons  
 224 increased with the solution temperature. This result confirmed that the solution temperature  
 225 enhanced the mass transfer phenomena and the diffusion of Cu<sup>2+</sup> ions inside the porous structure  
 226 of these adsorbents. Thus, the increment of this quantity was associated with the number of  
 227 adsorbed ions per functional group and the adsorption energy. Comparatively, the AC CO<sub>2</sub>-  
 228 Lemon-RLP adsorbent showed the highest Cu<sup>2+</sup> removal and was the most effective for this  
 229 purpose. Furthermore, characterization results reported in (Dotto et al. 2011) indicated that  
 230 the acidic functionalities of these activated carbons were responsible for Cu<sup>2+</sup> removal. In  
 231 particular, FTIR analysis of activated carbon samples before and after Cu<sup>2+</sup> adsorption indicated  
 232 that the main acidic functional groups were OH and COOH. The absorption bands relative to  
 233 these groups presented significant shifts after Cu<sup>2+</sup> adsorption thus suggesting that OH and  
 234 COOH were involved in the interactions with Cu<sup>2+</sup> ions, and confirming the statistical physics  
 235 calculations.

236 For illustration, Table 2 shows the  $\text{Cu}^{2+}$  adsorption capacities for different activated  
 237 carbons reported in the literature. It was clear that these activated carbons can be an alternative  
 238 to remove the  $\text{Cu}^{2+}$  ions from wastewaters and to contribute to the reduction of solid waste  
 239 generation. They can also outperform other adsorbents reported in the literature. For instance,  
 240 the  $\text{Cu}^{2+}$  adsorption capacities of 1-iron-modified flaxseed waste, sodium dodecyl sulfate  
 241 modified iron pillared montmorillonite, and activated carbons functionalized with magnetic  
 242 iron oxide nanoparticles were 7.64, 20.6, and 41.6 mg/g (Li and Wu 2010; Gu et al. 2019;  
 243 Cerrahoğlu Kaçakgil and Çetintaş 2021).

244  
 245 **Table 2.**  $\text{Cu}^{2+}$  adsorption capacities of activated carbons obtained from different  
 246 feedstock (Mariana et al. 2021).

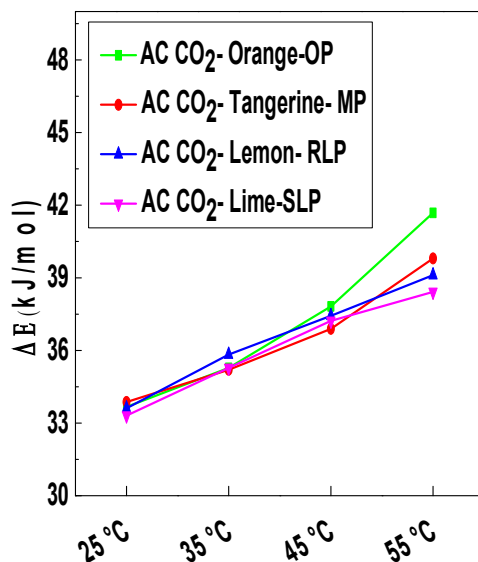
Preparation conditions			
Feedstock	Temperature, °C	Time, min	Adsorption capacity, mg/g
Cauliflower leaves	600	120	75.99
Ginkgo leaf	800	90	310.0
Pinewood sawdust	700	120	419.1

247  
 248  
 249 *3.3.  $\text{Cu}^{2+}$  adsorption energy*  
 250  
 251 Adsorption energy for the interaction  $\text{Cu}^{2+}$  ion-activated carbon surface was determined from  
 252 the concentration values at half-saturation and the following equation (Dhaouadi et al. 2021):  
 253

$$254 \quad \Delta E_{\text{int}(FG-\text{Cu}^{2+})} = RT \ln \frac{C_s}{C_{1/2}} \quad (4)$$

255

256 where  $R=8.314$  J/mol·K is the ideal gas constant, and  $C_s$  is the copper solubility. The adsorption  
257 energy for the interaction of acidic functional groups of these activated carbons and  $\text{Cu}^{2+}$  ions is  
258 depicted in Figure 4.



259

260 **Figure 4:** Calculated  $\text{Cu}^{2+}$  adsorption energies for tested activated carbons.

261

262 All interaction energy values were lower than 40 kJ/mol, thus suggesting that this  
263 adsorption process was associated with physical forces. As stated, the acidic functional groups  
264 (e.g., OH and COOH) of these activated carbons were involved in the  $\text{Cu}^{2+}$  adsorption.  
265 Furthermore, this adsorption energy increased with solution temperature for all activated  
266 carbons.

267

#### 268 4. Conclusions

269

270 A reliable modeling of adsorption data and the corresponding analysis of adsorption  
271 mechanism are paramount for the design of water treatment processes effective to remove heavy

272 metals with activated carbons. Therefore, this study reports the statistical physics-based  
273 interpretation of  $\text{Cu}^{2+}$  adsorption using four activated carbons obtained from citrus wastes,  
274 which are low-cost feedstock to prepare new adsorbents. Steric and energetic parameters were  
275 calculated for the adsorption of this heavy metal using a monolayer adsorption model. Results  
276 showed that the  $\text{Cu}^{2+}$  adsorption was multi-cationic via one functional group (i.e., acidic surface  
277 functionalities). In addition,  $\text{Cu}^{2+}$  adsorption was endothermic and associated with physical  
278 interaction forces. At saturation,  $\text{Cu}^{2+}$  adsorption capacities ranged from 54.6 to 87.9 mg/g for  
279 these activated carbons. Finally, this advanced modeling provided interesting interpretations of  
280 the adsorption mechanism of this relevant water pollutant with low-cost activated carbons.

281

## 282 **Acknowledgements**

283

284 Sonia Taamalli, Florent Louis, and Abderrahman El Bakali appreciated the support from the  
285 LABEX CaPPA (Chemical and Physical Properties of the Atmosphere), which is funded by the  
286 French National Research Agency (ANR) through the PIA  
287 (Programmed'Investissement d'Avenir) under contract ANR-11-LABX-0005-01 and also the  
288 Regional Council "Hauts de France" and the "European Funds for Regional Economic  
289 Development.

290 **-Ethical Approval:** Not applicable

291 **-Consent to Participate:** Not applicable.

292 **-Consent to Publish:** Not applicable.

293 **-Author Contributions: Conceptualization:** Lotfi Sellaoui, Abdemottaleb Ben Lamine,

294 **Methodolog:** Kátia da Boit Martinello, Fatma Dhaouadi, Michael Badawi, Adrián Bonilla-

295 Petriciolet, Luis Felipe Oliveira Silva, Guilherme Luiz Dotto, Sonia Taamalli



296 **Writing - original draft preparation:** LotfiSellaoui, Fatma Dhaouadi, Florent Louis,  
297 Abderrahman El Bakali

298 **Supervision:** LotfiSellaoui

299 **-Funding:** Not applicable

300 **-Competing Interests:** The authors declare that they have no competing interests

301 **-Availability of data and materials:** Note applicable

## 302 **References**

303

304 Anbazhagan S, Thiruvengadam V, Sukeri A (2021) An Amberlite IRA-400 Cl<sup>-</sup> ion-exchange  
305 resin modified with Prosopis juliflora seeds as an efficient Pb<sup>2+</sup> adsorbent: adsorption,  
306 kinetics, thermodynamics, and computational modeling studies by density functional  
307 theory. RSC Adv 11:4478–4488. <https://doi.org/10.1039/D0RA10128A>

308 Bell JG, Zhao X, Uygur Y, Thomas KM (2011) Adsorption of Chloroaromatic Models for  
309 Dioxins on Porous Carbons: The Influence of Adsorbate Structure and Surface  
310 Functional Groups on Surface Interactions and Adsorption Kinetics. J Phys Chem C  
311 115:2776–2789. <https://doi.org/10.1021/jp1099893>

312 Cerrahoğlu Kaçakgil E, Çetintaş S (2021) Preparation and characterization of a novel  
313 functionalized agricultural waste-based adsorbent for Cu<sup>2+</sup> removal: Evaluation of  
314 adsorption performance using response surface methodology. Sustainable Chemistry  
315 and Pharmacy 22:100468. <https://doi.org/10.1016/j.scp.2021.100468>

316 Dhaouadi F, Sellaoui L, Badawi M, Reynel-Ávila H E, Mendoza-Castillo D I, Jaime-Leal J  
317 E, Bonilla-Petriciolet A, Lamine A B (2020a) Statistical physics interpretation of the  
318 adsorption mechanism of Pb<sup>2+</sup>, Cd<sup>2+</sup> and Ni<sup>2+</sup> on chicken feathers. Journal of  
319 Molecular Liquids 319:114168. <https://doi.org/10.1016/j.molliq.2020.114168>

320 Dhaouadi F, Sellaoui L, Chávez-González B, Elizabeth Reynel-Ávila H, Diaz-Muñoz L  
321 L, Mendoza-Castillo D I, Bonilla-Petriciolet A, Lima E C, Tapia-Picazo J C, Lamine A  
322 B (2020b) Application of a heterogeneous physical model for the adsorption of Cd<sup>2+</sup>,  
323 Ni<sup>2+</sup>, Zn<sup>2+</sup> and Cu<sup>2+</sup> ions on flamboyant pods functionalized with citric acid.  
324 Chemical Engineering Journal 127975. <https://doi.org/10.1016/j.cej.2020.127975>

325 Dhaouadi F, Sellaoui L, Dotto GL, Bonilla-Petriciolet A, Erto A, Lamine A B (2020c)  
326 Adsorption of methylene blue on comminuted raw avocado seeds: Interpretation of the  
327 effect of salts via physical monolayer model. Journal of Molecular Liquids 305:112815.  
328 <https://doi.org/10.1016/j.molliq.2020.112815>

329 Dhaouadi F, Sellaoui L, Reynel-Ávila HE, Landín-Sandoval V, Mendoza-Castillo D I, Jaime-  
330 Leal J E, Lima E C, Bonilla-Petriciolet A, Lamine A B (2021) Adsorption mechanism  
331 of Zn<sup>2+</sup>, Ni<sup>2+</sup>, Cd<sup>2+</sup>, and Cu<sup>2+</sup> ions by carbon-based adsorbents: interpretation of  
332 the adsorption isotherms via physical modelling. Environ Sci Pollut Res.  
333 <https://doi.org/10.1007/s11356-021-12832-x>

334 Dotto GL, Vieira MLG, Gonçalves JO, Pinto LA de A (2011) Removal of acid blue 9, food  
335 yellow 3 and FD&C yellow no 5 dyes from aqueous solutions using activated  
336 carbon, activated earth, diatomaceous earth, chitin and chitosan: equilibrium studies and  
337 thermodynamic. Química Nova 34:1193–1199

338 Dou J, Gan D, Huang Q, Chen J, Deng F, Zhu X, Wen Y, Zhang X, Wei Y (2019)  
339 Functionalization of carbon nanotubes with chitosan based on MALI multicomponent  
340 reaction for Cu<sup>2+</sup> removal. International Journal of Biological Macromolecules  
341 136:476–485. <https://doi.org/10.1016/j.ijbiomac.2019.06.112>

342 Godiya CB, Cheng X, Li D, Chen Z, Lu X (2019) Carboxymethyl cellulose/polyacrylamide  
343 composite hydrogel for cascaded treatment/reuse of heavy metal ions in wastewater.

344 Journal of Hazardous Materials 364:28–38.  
345 <https://doi.org/10.1016/j.jhazmat.2018.09.076>

346 Gu S-Y, Hsieh C-T, Gandomi YA, Yang Z F, Li L, Fu C C, Juang R S (2019) Functionalization  
347 of activated carbons with magnetic Iron oxide nanoparticles for removal of copper ions  
348 from aqueous solution. Journal of Molecular Liquids 277:499–505.  
349 <https://doi.org/10.1016/j.molliq.2018.12.018>

350 Katiyar R, Patel AK, Nguyen T-B, Singhania R R, Chen C W, Dong C D(2021) Adsorption of  
351 copper (II) in aqueous solution using biochars derived from *Ascophyllum nodosum*  
352 seaweed. Bioresource Technology 328:124829.  
353 <https://doi.org/10.1016/j.biortech.2021.124829>

354 Kayalvizhi K, Alhaji NMI, Saravanakkumar D, Mohamed S B, Kaviyarasu K, Ayeshamariam  
355 A, Al-Mohaimed A M, Abdel Gawwad M R, Elshikh M S (2022) Adsorption of copper and  
356 nickel by using sawdust chitosan nanocomposite beads – A kinetic and thermodynamic  
357 study. Environmental Research 203:111814.  
358 <https://doi.org/10.1016/j.envres.2021.111814>

359 Khan J, Lin S, Nizeyimana JC, Wu Y, Wang Q, Liu X (2021) Removal of copper ions from  
360 wastewater via adsorption on modified hematite ( $\alpha$ -Fe<sub>2</sub>O<sub>3</sub>) iron oxide coated sand.  
361 Journal of Cleaner Production 319:128687.  
362 <https://doi.org/10.1016/j.jclepro.2021.128687>

363 Lam SS, Liew RK, Cheng CK, Rasit N, Ooi C K, Ma N L, Ng J H, Lam W H, Chong C T,  
364 Chase H A (2018) Pyrolysis production of fruit peel biochar for potential use in  
365 treatment of palm oil mill effluent. Journal of Environmental Management 213:400–  
366 408. <https://doi.org/10.1016/j.jenvman.2018.02.092>

367 Lam SS, Liew RK, Lim XY, Ani F N, Jusoha A (2016) Fruit waste as feedstock for recovery  
368 by pyrolysis technique. *International Biodeterioration & Biodegradation* 113:325–333.  
369 <https://doi.org/10.1016/j.ibiod.2016.02.021>

370 Lemes LFR, Tarley CRT (2021) Combination of supramolecular solvent-based microextraction  
371 and ultrasound-assisted extraction for cadmium determination in flaxseed flour by  
372 thermospray flame furnace atomic absorption spectrometry. *Food Chemistry*  
373 357:129695. <https://doi.org/10.1016/j.foodchem.2021.129695>

374 Li S-Z, Wu P-X (2010) Characterization of sodium dodecyl sulfate modified iron pillared  
375 montmorillonite and its application for the removal of aqueous Cu(II) and Co(II).  
376 *Journal of Hazardous Materials* 173:62–70.  
377 <https://doi.org/10.1016/j.jhazmat.2009.08.047>

378 Mariana M, H.P.S. AK, Mistar EM, Yahya EB, Alfatah T, Danish M, Amayreh M (2021)  
379 Recent advances in activated carbon modification techniques for enhanced heavy metal  
380 adsorption. *Journal of Water Process Engineering* 43:102221.  
381 <https://doi.org/10.1016/j.jwpe.2021.102221>

382 Nyström F, Nordqvist K, Herrmann I, Nordqvist K, Herrmann I, Hedström A, Viklander M  
383 (2020) Removal of metals and hydrocarbons from stormwater using coagulation and  
384 flocculation. *Water Research* 182:115919.  
385 <https://doi.org/10.1016/j.watres.2020.115919>

386 Pan J, Gao Y, Gao B, Guo K, Xu X, Yue Q (2019) One-step synthesis of easily-recoverable  
387 carboxylated biogas residues for efficient removal of heavy metal ions from synthetic  
388 wastewater. *Journal of Cleaner Production* 240:118264.  
389 <https://doi.org/10.1016/j.jclepro.2019.118264>

390 Perondi D, Poletto P, Restelatto D, Manera C, Silva JP, Junges J, Collazzo GC, Dettmer A,  
391 Godinho M, Vilela ACF(2017) Steam gasification of poultry litter biochar for bio-  
392 syngas production. *Process Safety and Environmental Protection* 109:478–488.  
393 <https://doi.org/10.1016/j.psep.2017.04.029>

394 Rukayat OO, Usman MF, Elizabeth OM, Abosede O O, Faith I U (2021) Kinetic Adsorption  
395 of Heavy Metal (Copper) On Rubber (Hevea Brasiliensis) Leaf Powder. *South African*  
396 *Journal of Chemical Engineering* 37:74–80. <https://doi.org/10.1016/j.sajce.2021.04.004>

397 Sellaoui L, Soetaredjo FE, Ismadji S, Benguerba Y, Dotto G L, Bonilla-Petriciolet A, Rodrigues  
398 A E, Ben Lamine A, Erto A (2018) Equilibrium study of single and binary adsorption  
399 of lead and mercury on bentonite-alginate composite: Experiments and application of  
400 two theoretical approaches. *Journal of Molecular Liquids* 253:160–168.  
401 <https://doi.org/10.1016/j.molliq.2018.01.056>

402 Sun H, Ji Z, He Y, Wang L, Zhan J, Chen L, Zhao Y (2022) Preparation of PAMAM modified  
403 PVDF membrane and its adsorption performance for copper ions. *Environmental*  
404 *Research* 204:111943. <https://doi.org/10.1016/j.envres.2021.111943>

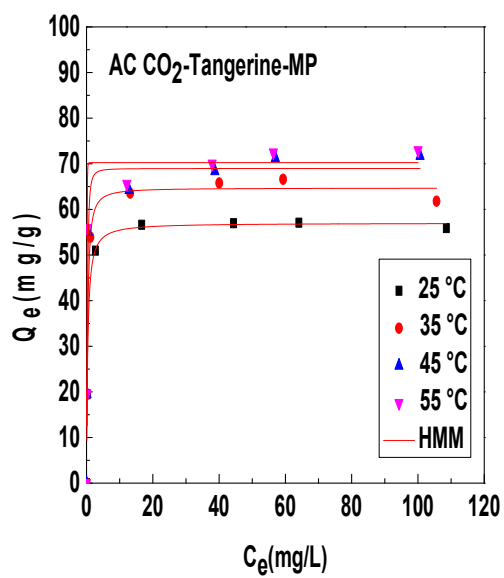
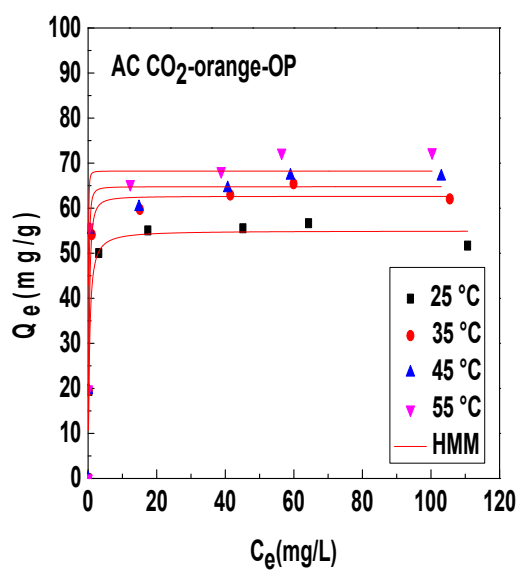
405 Voccianti M, Trofa M, Rodríguez-Estupiñán P, Giraldo L, D’Auria T, Moreno-Piraján J C,  
406 Erto A(2014) A rigorous procedure for the design of adsorption units for the removal of  
407 cadmium and nickel from process wastewaters. *Journal of Cleaner Production* 77:35–  
408 46. <https://doi.org/10.1016/j.jclepro.2013.12.001>

409

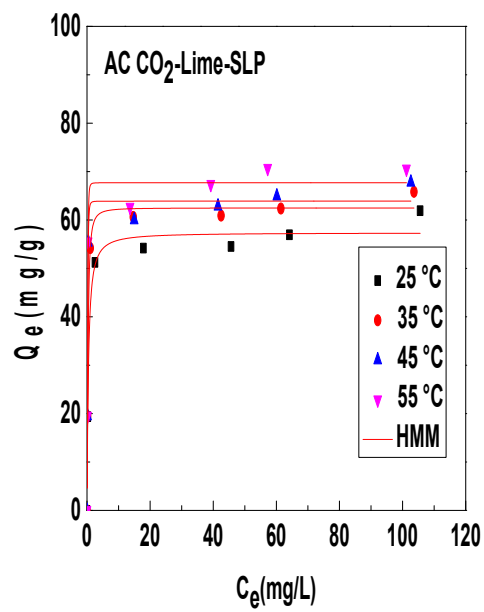
410

## 411 **Appendix**

412 The fitting data results of the experimental isotherms of  $\text{Cu}^{2+}$  ions are given below:



413



414

415

416